ACS APPLIED MATERIALS & INTERFACES

Research Article

www.acsami.org

TiO_2@CeO_x Core–Shell Nanoparticles as Artificial Enzymes with Peroxidase-Like Activity

Luca Artiglia,[†] Stefano Agnoli,*[,†] Maria Cristina Paganini,[‡] Mattia Cattelan,[†] and Gaetano Granozzi[†]

[†]Department of Chemical Sciences, University of Padova, via Marzolo 1, I-35131 Padova, Italy

[‡]Department of Chemistry, University of Torino, via Giuria 7, 10125 Torino, Italy

Supporting Information

ABSTRACT: The Ce^{4+}↔ Ce^{3+} redox switch is at the basis of an all-inorganic catalytic cycle that is capable of mimicking the activity of several natural redox enzymes. The efficiency of these artificial enzymes (nanozymes) strongly depends on the Ce^{4+}/Ce^{3+} ratio. By capitalizing on the results obtained on oxide/oxide model systems, we implemented a simple and effective procedure to obtain conformal TiO_2@CeO_x core–shell nanoparticles whose thickness is controlled with single-layer precision. Since the Ce^{3+} species are stabilized only at the interface by the electronic hybridization with the TiO_2 states, the modulation of the shell thickness offers a simple method to tailor the Ce^{4+}/Ce^{3+} ratio and therefore the catalytic properties. The activity of these nanoparticles as artificial peroxidase-like enzymes was tested, showing exceptional performances, even better than natural horseradish peroxidase enzyme. The main advantage with respect to other oxide/oxide nanozymes is that our nanoparticles, having a tunable Ce^{4+}/Ce^{3+} ratio, are efficient already at low H_2O_2 concentrations.

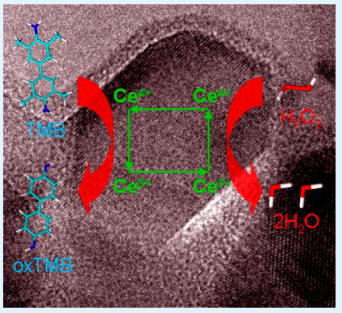

KEYWORDS: *titanium dioxide, cerium oxide, interface hybridization, core–shell, artificial enzyme, peroxidase*

INTRODUCTION

Cerium oxide, CeO_2, is one of the most interesting oxides in catalysis, being an efficient catalyst itself or a subtle structural and electronic promoter in several chemical processes.[1−5] The key point at the basis of its catalytic activity is the low energy cost for the formation of oxygen vacancies and Ce^{3+} centers. Since these chemical species are extremely catalytically active, a huge amount of studies have focused on the strategies to maximize their amount, stability, and organization. Among the several processes that are controlled by ceria defects, the oxygen activation is maybe the most important since it impacts very different chemical fields, such as high-yield industrial reactions and fine chemical and even biological syntheses.[6−8] Actually, the Ce^{4+}↔Ce^{3+} redox switch is the all-inorganic analogue of the catalytic cycle of redox enzymes[9−13] where metal centers are used as cofactors to promote reversible redox reactions and/or against intracellular oxidative stress[14−16] in cell metabolism.

So far, several strategies have been used to manipulate the Ce^{4+}/Ce^{3+} ratio, such as reduction in the geometrical size,[17,18] introduction of dopants or other oxides, and kinetically controlled synthesis.[19−22] The outcomes of these works have demonstrated that the presence of defects enhances significantly the reactivity, although in many cases, defects are metastable, and their chemical activity is lost as a consequence of nanoparticle (NP) coalescence and/or interaction with the reaction environment.

In this paper we propose a radically new approach, based on the creation of an oxide/oxide interface capable of providing a strong stabilization for defect centers. Following the blueprint outlined from theoretical[23] and experimental model studies,[24] the possibility emerges of stabilizing Ce^{3+} by the interfacial hybridization with a reducible oxide support. In the case of titania, by virtue of the electronic hybridization between the TiO_2 O 2p band and Ce 4f states, Ce^{3+} species are strongly stabilized with respect to unsupported ceria, allowing to obtain almost exclusively reduced species at the interface in a wide range of experimental conditions.[23,25,26] Interestingly, the localized nature of electronic hybridization determines that the stabilization of reduced states is sensibly thickness-dependent. Recently, it has been demonstrated that when the CeO_x coverage exceeds the monolayer, the interface hybridization is progressively lost, so that stoichiometric CeO_2 starts to grow.[24] This opens the way to the control of the Ce^{4+}/Ce^{3+} ratio simply by choosing the thickness of the ceria shell supported on TiO_2.

Taking the cue from this vision, in the following work we optimized a synthetic protocol based on atomic layer deposition of an organometallic Ce^{3+} precursor on a commercial TiO_2 powder suspension, with the aim of obtaining a of single layer of CeO_x on TiO_2, and therefore preparing thickness-controlled TiO_2@CeO_x core–shell NPs. The activity as a peroxidase-like enzyme of core–shell NPs with different Ce^{4+}/Ce^{3+} ratios was tested by means of a biomimetic assay.

The success of this synthesis scheme indicates that the use of core–shell nanoparticles bearing controlled interfaces represents a suitable approach for the realization of nanostructures with specific functionalities. Actually, with respect to standard

Received: August 25, 2014
Accepted: October 16, 2014
Published: October 16, 2014

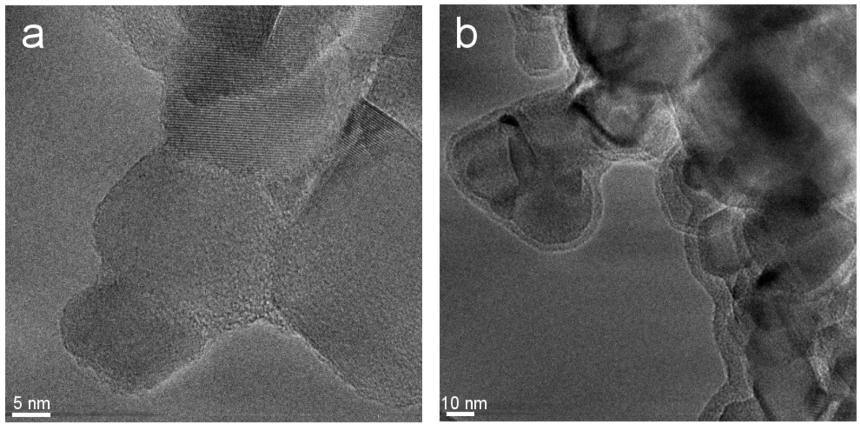

Figure 1. TEM Images of TiO_2@CeO_x samples: (a) **TC1** (400 000×) and (b) **TC3** (150 000×). The conformal growth of ceria, indicative of a layer-by-layer growth, is evident from the huge homogeneity and perfectly wetting behavior of the outer shell surrounding the TiO_2 nanocrystals.

nanoparticles (e.g., simple nanoceria), core−shell systems can be designed to combine the bulk properties of the core (e.g., magnetism, light adsorption or emission) with very specific chemical properties of the shell, so that the resulting system can exhibit multiple functions.[27,28] Moreover the strong electronic stabilization intrinsic to the formation of the oxide/oxide interface provides an effective strategy to promote biocompatibility and to enhance chemical stability in harsh conditions.

MATERIALS AND METHODS

Synthesis of the TiO_2@CeO_x (TC) Core−Shell NPs. The core−shell samples were obtained by impregnation of a commercial TiO_2 powder (Degussa Aeroxide© P25) in a cerium(III) 2-ethylhexanoate (49% in 2-ethylhexanoic acid, Alfa Aesar) precursor solution.[29] The TiO_2 powder was pretreated at 570 K in air to remove any residual water and then added to a 0.75 mol/L solution of the precursor in *n*-hexane at room temperature (thermostatic bath). The mixture was stirred for 5 h; afterward, the powder was filtered and washed with *n*-hexane to remove any precursor residue. The product was dried and then calcined at 920 K (heating ramp of 5 K/min) in air for 8 h.

Structural and Functional Characterization. Transmission electron microscopy (TEM) analysis of the powder samples deposited on a copper grid was performed in Torino, using a Jeol JEM 3010 (300 kV) microscope equipped with an EDS detector by Oxford Instruments.

X-ray photoelectron spectroscopy (XPS) spectra were collected in Padova in an ultrahigh vacuum chamber (base pressure 1.0×10^{-9} mbar) equipped with a VG MKII Escalab electron analyzer. Photoemission spectra were taken at room temperature in normal emission using a nonmonochromatized Al anode X-ray source ($h\nu$ = 1486.6 eV). Powder samples were suspended in bidistilled water and drop-casted on high-purity copper foils. After drying in air the obtained films were introduced into the ultrahigh vacuum chamber and outgassed overnight. The charging observed during measurements was corrected using adventitious carbon as the internal reference. Raman spectra were acquired with a ThermoFisher DXR Raman microscope, using a 532 nm laser (5.0 mW) focused on the sample with a 50× objective (Olympus) to obtain a spot size of about 1 μm.

For peroxidase-like kinetic assays, 3,3′,5,5′-tetramethylbenzidine (TMB) was purchased from Sigma-Aldrich. All the tests were performed in a pH = 4 citrate buffer using different concentrations of either TMB or H_2O_2 (35%, Sigma-Aldrich) and 200 μg/mL of TC samples powder.

The peroxidase-like reaction, catalyzed by TC powders, is the following:

$$\mathrm{TMB(aq)} + \mathrm{H_2O_2(aq)} \rightarrow \mathrm{oxTMB(aq)} + 2\mathrm{H_2O(l)}$$

This reaction follows a ping-pong mechanism in which 3,3′,5,5′-tetramethybenzidine (TMB, transparent solution) is oxidized to 3,3′,5,5′-tetramethylbenzidine diimine (oxTMB, blue solution) and H_2O_2 is reduced to H_2O.

As long as the reaction proceeds, and TMB is oxidized to oxTMB, the solution turns to blue (see Supporting Information, Figure S1); thus, the kinetics can be monitored acquiring the oxTMB absorbance peak, centered at λ = 652 nm. The UV−vis spectra were collected at 120 s steps in a Varian Cary-50 spectrometer, with a scan rate of 600 nm/min.

RESULTS AND DISCUSSION

Synthesis and Characterization of Core−Shell NPs. CeO_x nanostructures, where Ce^{3+} species are stabilized by the interaction with the substrate, were grown on TiO_2 in ideal conditions (ultrahigh vacuum) by physical vapor deposition of a controlled amount of metallic Ce (electron beam evaporation from a metallic Ce target) in controlled oxygen environments, followed by thermal treatment.[24] Nevertheless, a simpler and highly scalable synthetic route, characterized by the same level of accuracy in the shell thickness, can be followed by taking advantage of the surface hydroxyl species on the TiO_2 support, which can be exploited to promote a surface sol−gel reaction with the Ce organometallic precursor. This reaction eventually leads to a Ti−O−Ce−$(OR)_x$ layer, whose organic component is removed during the calcination. Cerium(III) 2-ethylhexanoate was chosen due to the steric protection of the metallic center, and the reaction was carried out in anhydrous conditions (anhydrous *n*-hexane solvent) to avoid any Ce^{3+} oxidation during the impregnation. In the following we will discuss the behavior of two samples obtained after

(i) a single impregnation (5 h in 0.75 mol/L *n*-hexane solution of the Ce precursor) + calcination (8 h at 920 K in air) step (named **TC1**);
(ii) three consecutive impregnation steps (5 h in 0.75 mol/L *n*-hexane solution of the Ce precursor) + calcination (8 h at 920 K in air) steps (named **TC3**).

We report the TEM images of **TC1** and **TC3** in Figure 1a,b, respectively. In the former case, it is possible to observe the typical TiO_2 crystal shape, whose edges are outlined by a very thin darker border due to the presence of ceria, as confirmed by EDX measurements (see Supporting Information, Table S1).

By repeating three times the impregnation + calcination procedure (**TC3**), a thicker layer (1−1.5 nm; i.e., ca. 3 ML) of amorphous ceria covers conformally the titania nanocrystals,

evidencing a layer by layer growth mode. Lower magnification TEM images (100 000×) of **TC1** and **TC3** are reported in Supporting Information, Figures S2 and S3, respectively. Supporting Information, Figure S3 demonstrates that all the NPs are uniformly covered by the CeO_x shell. An evaluation of the NPs average dimension gave 22.8 ± 0.3 nm for **TC1** and 25.9 ± 0.9 nm for **TC3**. Such an increase could be due to the multiple heating treatments at 920 K performed on the latter.

XPS data of the Ce 3d core levels are displayed in Figure 2. The photoemission spectrum of a CeO_2 nanopowder, taken as

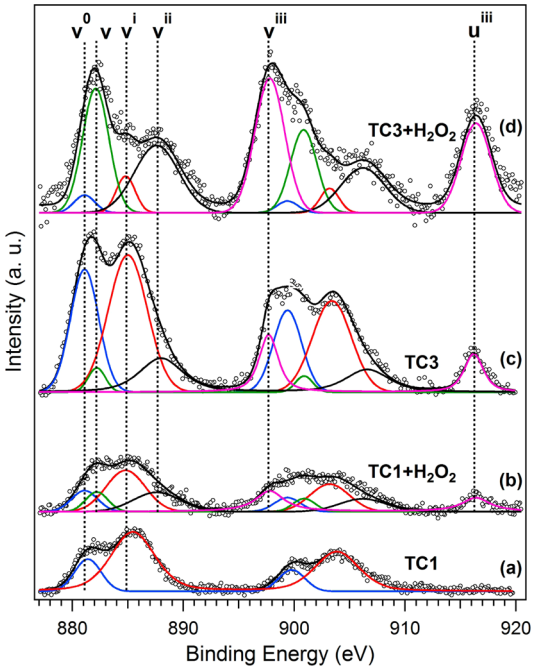

Figure 2. XPS Ce 3d data of the TiO_2@CeO_x powders obtained after calcination, (a) **TC1**, (c) **TC3**, and after reaction in a 0.058 M H_2O_2 solution, (b) **TC1**, (d) **TC3**.

a reference (see Figure S4 in Supporting Information), shows the three typical spin−orbit-split doublets corresponding to the different 4f configurations in the photoemission final state.[24,30] The component labeled u^{iii} at 916.3 eV is indicative of the poorly screened Ce $3d^94f^0$ O $2p^6$ final state, connected with the presence of Ce^{4+} ions. The XPS data of **TC1** and **TC3** strongly differ from the reference CeO_2. The former (Figure 2a) shows only two peaks at 881.1 and 885.0 eV (labeled as v^0 and v^i, respectively), replicated by spin−orbit-splitting satellites (18.2 eV), which can be ascribed to Ce $3d^94f^2$ O $2p^5$ and Ce $3d^94f^1$ O $2p^6$ final states, respectively. These findings, combined with the absence of the u^{iii} peak, reveal the almost exclusive presence of Ce^{3+} ions, confirming that one monolayer of ceria is stabilized in the reduced state by the interaction with TiO_2. On the contrary, the XPS data corresponding to **TC3** (Figure 2c) differ from those of **TC1**, showing a change in the relative intensity between the different components and the presence of the u^{iii} satellite. Therefore, the **TC3** XPS data are representative of an oxide whose composition is an "average" between stoichiometric CeO_2 and **TC1**. A multipeak analysis of the 3d photoemission peaks (Figure 2c) allows a quantification of the Ce^{3+} (v^0, v^i) and Ce^{4+} (v, v^{ii}, v^{iii}) components (72% Ce^{3+} and 28% Ce^{4+}).[31]

Raman spectroscopy is another powerful technique to evaluate the presence of CeO_x, the structure of the TiO_2 support (anatase and rutile have a characteristic Raman fingerprint), and a possible interaction between the two.[21,32,33] Raman spectra of the **TC1** and **TC3** samples, together with TiO_2 P25 and CeO_2 (nanopowder, Aldrich), are reported in Figure 3. In the case of **TC1**, no clear peak related

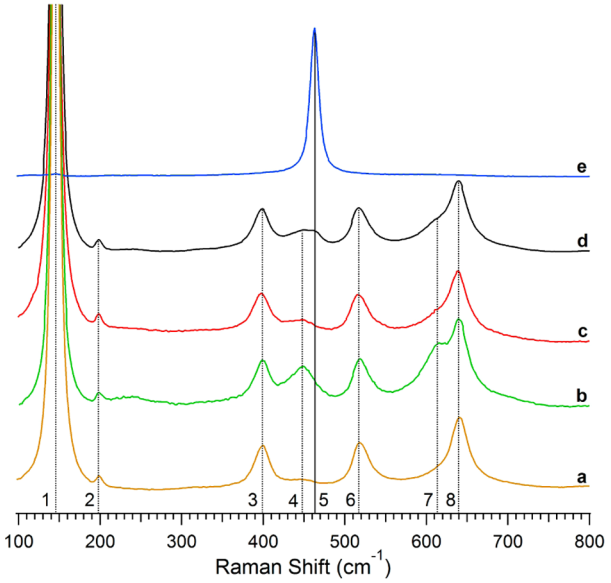

Figure 3. Raman spectra of (a) TiO_2 P25 powder, (b) TiO_2 P25 powder after 8h calcination at 920 K, (c) **TC1**, (d) **TC3**, (e) CeO_2 nanopowder.

Table 1. Assignment of the Raman Peaks

phase	wavenumber (cm^{-1})	assignment[a]
anatase	144−147	1
	198	2
	398	3
	515	6
	640	8
rutile	448	4
	612	7
CeO_2	463	5

[a]See Figure 3.

to CeO_x can be detected (peak 5, see Table 1), probably due to the small amount of the oxide and the overlap with peak 4 coming from the TiO_2 support. On the contrary, the **TC3** spectrum displays a double peak in the 410−480 cm^{-1} range: the peak at higher frequency (463 cm^{-1}) is due to CeO_x, while the low-frequency one (448 cm^{-1}) is typical of the TiO_2 support (rutile band).

An interesting evidence of the TiO_2−CeO_x interaction emerges from the comparison between the spectra of TC and pure TiO_2−P25. The green curve in Figure 3 refers to a TiO_2 P25 powder subjected to the same annealing as the TC samples (8 h calcination at 920 K in air). As a result of this treatment, rutile peaks (labeled 4 and 7) become very intense. The same peaks are also present in the TC samples (the TiO_2−P25 support itself contains about 20% rutile and 80% anatase) and in the TiO_2 P25 powder without thermal treatment (orange curve in Figure 3), but their intensity with respect to anatase (the spectra a,b and c have been normalized to peak 1, which

dx.doi.org/10.1021/am5057129 | ACS Appl. Mater. Interfaces 2014, 6, 20130−20136

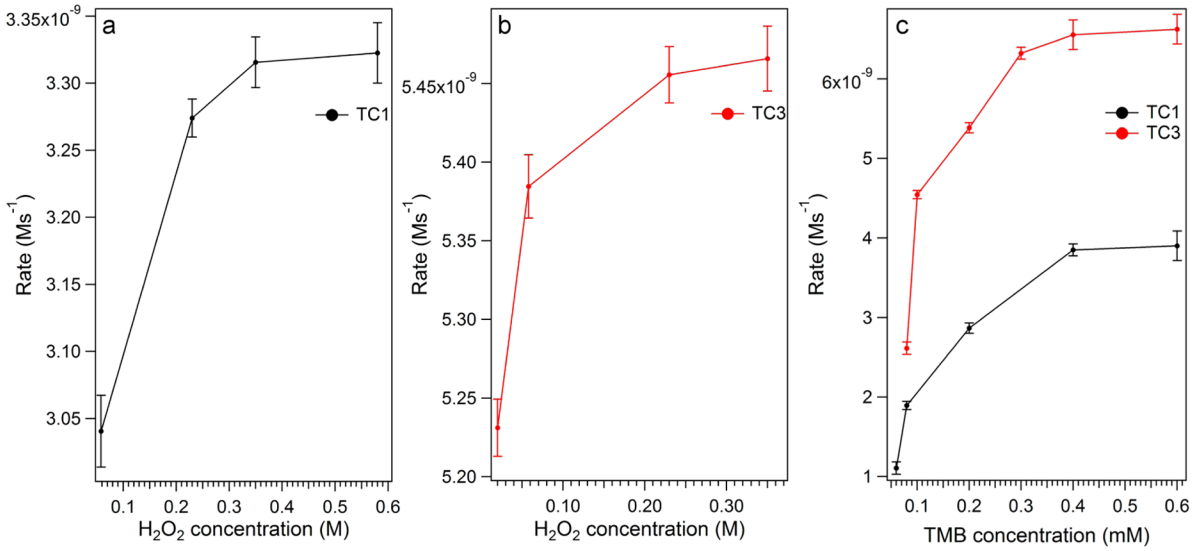

Figure 4. Reaction rate of **TC1** (a) and **TC3** (b) samples at different $[H_2O_2]$ ($[TMB] = 0.2$ mM) and (c) reaction rate of TC samples as a function of $[TMB]$ ($[H_2O_2] = 0.058$ M).

corresponds to B_{1g} and E_g vibration modes)[32] is strongly quenched. Previous Raman and X-ray diffraction studies demonstrate that, when CeO_2 grows in contact with TiO_2–anatase, it inhibits the anatase to rutile conversion up to 1000 K through the formation of interfacial Ce–O–Ti bonds.[34] On the other hand, in pure TiO_2 the phase transition between the two polymorphs is thermodynamically favored above 870 K, which explains the intense rutile peaks observed in the Raman spectrum of clean TiO_2 P25 annealed at 920 K (Figure 3, green curve).[35] Therefore, Raman provides a further evidence of the strong interaction between TiO_2 and CeO_x in TC samples. Moreover oxide intermixing, which would lead to the formation of a cerium titanate ($Ce_2Ti_2O_7$) phase as observed in some ceria-titania composites obtained by sol–gel synthesis,[21] can be ruled out because its typical Raman lines (at 168, 197, 275, 326, 362, 456, 560, and 631 cm^{-1})[21,36] were not observed.

Thence, **TC3** is a TiO_2@CeO_x core–shell where Ce^{3+} ions, stabilized at the interface with TiO_2, and fully oxidized Ce^{4+} ions are copresent. Moreover, the stabilization of Ce^{3+} species does not depend on extrinsic factors, such as nanodimension or metastable state obtained during a kinetically driven synthesis, but on an electronic interaction that is unaffected by ambient conditions.

Reactivity of Core–Shell NPs as Artificial Enzymes. Being able to synthesize ceria-coated NPs characterized by a tunable amount of Ce^{4+}/Ce^{3+} but identical in terms of structure, morphology, dimensions, and surface area, we decided to investigate how defectivity impacts their activity as artificial enzymes. Recently, ceria NPs with different Ce^{4+}/Ce^{3+} ratios showed the ability to act as mimics of superoxide dismutase, catalase, and oxidase, thus proving to be efficient artificial enzymes (often referenced as nanozymes)[37] able to protect cells from the oxidative stress due to an excess of reactive oxygen species.[9−13,38,39] In a recent work, Peng et al.[33] asserted that CeO_2 NPs, instead of working as a catalyst, behave as an oxidizing agent, due to the progressive dissolution of Ce^{3+} in the reactive mixture. Therefore, a good strategy to prevent this leaching is to stabilize the Ce^{3+} active sites, allowing CeO_x to run like a catalyst.

As a case study, we investigated the activity of TiO_2@CeO_x as a peroxidase-like enzyme using standard colorimetric tests based on 3,3′,5,5′-tetramethylbenzidine (TMB) oxidation. Similarly to the horseradish peroxidase (HRP) natural enzyme, CeO_2 NP catalytic activity is dependent on the pH, temperature, and concentration of H_2O_2. In agreement with previous biomimetic assays, our tests were performed at 300 K and pH = 4.0 buffer.[13,33] Figure 4a,b shows the reaction rate for **TC1** and **TC3** as a function of the H_2O_2 substrate concentration, obtained at a fixed TMB concentration (0.2 mM). The reaction rate calculated using TMB as a substrate ($[H_2O_2] = 0.058$ M) is reported for both samples in Figure 4c.

On the basis of the data reported in Figure 4, in a wide range of TMB and H_2O_2 concentrations we could obtain the apparent Michaelis–Menten steady-state kinetic parameters to evaluate the peroxidase-like activity. The results (double reciprocal plots) are shown in Supporting Information, Figure S5. The first tests, obtained adding varied amounts of TMB to a solution of $[H_2O_2]$ at fixed concentration (0.058 M), show that **TC1** and **TC3** kinetic parameters are comparable (K_M^{app} = 0.28 and 0.30 mM, respectively, see Table 2), but lower with respect to HRP (0.43 mM),[40] denoting a good affinity for TMB, which is a common feature of all inorganic mimics of peroxidase, such as Fe_3O_4,[34] CuO,[41] and FeS.[42,43]

On the contrary, the affinity toward the oxidant is much scarcer. In general, nanozymes require a higher peroxide concentration than HRP to reach the maximum activity.[34,35,44] Interestingly, our core–shell NPs escape this trend. As a matter of fact, if H_2O_2 is tested as a substrate, by changing its concentration in the presence of 0.2 mM TMB the **TC1** K_M^{app} value increases by about 20 times, and its calculated value (6.29 mM) is higher than that measured for HRP;[34] however, the order of magnitude is smaller than it is for other oxides (CuO 85.6 mM, Fe_3O_4 154 mM, see Table 1)[34,35] and comparable with other highly efficient mimics (graphene oxide 3.99 mM, FeS 7.2 mM).[36,38] Surprisingly, also **TC3** shows an increase of the K_M^{app} (1.39 mM) but quite modest, smaller than the natural enzyme.

Therefore, the apparent kinetic parameters indicate an exceptional performance for **TC1** and especially for **TC3** samples as peroxidase-like enzymes, showing a strong affinity for TMB and, above all, for the oxidant molecule H_2O_2. This result is of paramount importance since the main limit of

Table 2. Apparent Kinetic Parameters Obtained from the Double Reciprocal Plots[a] Compared with the Natural Enzyme (HRP) and Other Artificial Enzymes

catalyst + substrate	K_M^{app} [mM]	V_{MAX}^{app} [nMs^{-1}]
TC1 + TMB	0.28 ± 0.03	6.5 ± 0.3
TC1 + H_2O_2	6.29 ± 0.94	34.0 ± 3.0
TC3 + TMB	0.30 ± 0.04	12.0 ± 0.6
TC3 + H_2O_2	1.39 ± 0.15	55 ± 5.0
HRP[34] + TMB	0.434	10.0
HRP[34] + H_2O_2	3.70	87.0
CuO[35] + TMB	0.013	
CuO[35] + H_2O_2	85.6	
Fe_3O_4[34] + TMB	0.098	34.4
Fe_3O_4[34] + H_2O_2	154	97.8
GO−COOH[38] + TMB	0.0237 ± 0.001	34.5 ± 3.1
GO−COOH[38] + H_2O_2	3.99 ± 0.67	38.5 ± 2.2
FeS[36] + TMB	0.13	
FeS[36] + H_2O_2	7.2	

[a]See Supporting Information, Figure S3.

inorganic mimics is their need for high concentration of H_2O_2 to work efficiently, which prevents their application in sensitive environments.[34,35] To rationalize the differences observed in the catalytic activity, we acquired the Ce 3d photoemission lines after the reaction of the TC samples with a 0.058 M solution of H_2O_2 (i.e., the same concentration used in the biomimetic assays). The resulting spectra (Figure 2b,d) show that both samples undergo a modification, due to the presence/increase of Ce^{4+} peaks after the reaction with the H_2O_2 solution. In particular, the multipeak analysis demonstrates that the relative percentage of the Ce^{4+} peaks (i.e., the sum of the v, v^{ii}, and v^{iii} multiplet/total Ce 3d area) passes from 0% to 50% for **TC1** and from 28% to 91% for **TC3**, indicating that **TC3** is more prone to oxidation than **TC1**. To test the morphological changes experienced by core−shell NPs in an oxidizing environment, we acquired TEM micrographs of a **TC3** sample after 12 h of immersion in a 0.058 M H_2O_2 solution. Supporting Information, Figure S6 shows that the shell roughness increases, probably because of quantitative Ce^{3+} oxidation at the CeO_x−TiO_2 interface and surface hydroxylation.

Therefore, if we assume a ping-pong mechanism for the TMB oxidation,[34] where initially the Ce^{3+}centers react with H_2O_2 with a consequent oxidation to Ce^{4+}, the lower affinity of the **TC1** toward the H_2O_2 substrate can be traced back to an excessive stabilization of Ce^{3+} sites at the interface with TiO_2, which hinders the redox switching of the Ce^{4+}/Ce^{3+} couple. Interestingly, the interfacial stabilization operated by TiO_2 not only changes quantitatively the Ce^{4+}/Ce^{3+} ratio, but also the very tendency of the reduced species to be oxidized.

CONCLUSION

Our results describe a procedure to obtain TiO_2@CeO_x NPs by a simple and well-reproducible impregnation technique. In this way it is possible to tune the thickness of the CeO_x shell and, by doing so, its oxidation state. In fact, in agreement with works on model systems,[24] Ce^{3+} ions are stabilized at the interface with TiO_2, and as long as the shell thickness is increased, it is possible to increase the Ce^{4+}/Ce^{3+} ratio. The electron shuttling between defects states (i.e., Ti 3d and Ce 4f bands) in heterointerfaces has demonstrated to be a totally general phenomenon that can be extended to other reducible oxides,[45−48] to stabilize active chemical species. This paves the way to a full gamut of core−shell nanoparticles characterized by enhanced chemical activity but that can also benefit from the intrinsic bulk properties of the core, which can be magnetic or optically active to implement in a single nanosystem multiple functionalities.

The activity of TiO_2@CeO_x as a peroxidase-like enzyme was tested by a colorimetric method employing TMB and H_2O_2. The apparent Michaelis−Menten kinetic parameters revealed that the shell thickness has a role in the catalyst activity. The **TC3** sample showed the best performances (in line or better than the natural HRP enzyme), that is, good affinity for TMB and, above all, for H_2O_2. Moreover, we demonstrated that the large hybridization between TiO_2 and CeO_x in **TC1** stabilizes exclusively Ce^{3+} at the interface, hindering its oxidation to Ce^{4+}. On the contrary, a 30%/70% ratio between Ce^{4+} and Ce^{3+} ions (**TC3**) promotes Ce^{3+} oxidation. Therefore, the interface not only changes quantitatively the number of reduced species, but also the intrinsic tendency of metal centers to accept or donates electrons. This provides a quite sophisticated and very general method to tune the redox switch of a catalytic cycle and to bring it in the conditions where the activity is maximized.[49,50]

ASSOCIATED CONTENT

Supporting Information

Additional TEM micrographs, with relative statistical analysis, photoemission spectra, and details about enzyme assays (double reciprocal plots). This material is available free of charge via the Internet at http://pubs.acs.org.

AUTHOR INFORMATION

Corresponding Author

*E-mail: stefano.agnoli@unipd.it.

Notes

The authors declare no competing financial interest.

ACKNOWLEDGMENTS

This work has been funded by the Italian Ministry of Instruction, University and Research (MIUR) through the FIRB Project RBAP115AYN "Oxides at the nanoscale: multifunctionality and applications". We thank Prof. P. Scrimin for useful discussion.

REFERENCES

(1) Senanayake, S. D.; Stacchiola, D.; Rodriguez, J. A. Unique Properties of Ceria Nanoparticles Supported on Metals: Novel Inverse Ceria/Copper Catalysts for CO Oxidation and the Water-Gas Shift Reaction. *Acc. Chem. Res.* **2013**, *46*, 1702−1711.

(2) Rodriguez, J. A.; Graciani, J.; Evans, J.; Park, J. B.; Yang, F.; Stacchiola, D.; Senanayake, S. D.; Ma, S. G.; Perez, M.; Liu, P.; Sanz, J. F.; Hrbek, J. Water-Gas Shift Reaction on a Highly Active Inverse CeO_x/Cu(111) Catalyst: Unique Role of Ceria Nanoparticles. *Angew. Chem., Int. Ed.* **2009**, *48*, 8047−8050.

(3) Fu, Q.; Saltsburg, H.; Flytzani-Stephanopoulos, M. Active Nonmetallic Au and Pt Species on Ceria-Based Water-Gas Shift Catalysts. *Science* **2003**, *301*, 935−938.

(4) Bunluesin, T.; Gorte, R. J.; Graham, G. W. Studies of the Water-Gas-Shift Reaction on Ceria-Supported Pt, Pd, and Rh: Implications for Oxygen-Storage Properties. *Appl. Catal., B* **1998**, *15*, 107−114.

(5) Li, H.; Lu, G.; Dai, Q.; Wang, Y.; Guo, Y.; Guo, Y. Hierarchical Organization and Catalytic Activity of High-Surface-Area Mesoporous Ceria Microspheres Prepared Via Hydrothermal Routes. *ACS Appl. Mater. Interfaces* **2010**, *2*, 838−846.

(6) Rao, G. R.; Fornasiero, P.; Di Monte, R.; Kaspar, J.; Vlaic, G.; Balducci, G.; Meriani, S.; Gubitosa, G.; Cremona, A.; Graziani, M. Reduction of NO over Partially Reduced Metal-Loaded CeO_2−ZrO_2 Solid Solutions. *J. Catal.* **1996**, *162*, 1−9.
(7) Esch, F.; Fabris, S.; Zhou, L.; Montini, T.; Africh, C.; Fornasiero, P.; Comelli, G.; Rosei, R. Electron Localization Determines Defect Formation on Ceria Substrates. *Science* **2005**, *309*, 752−755.
(8) Campbell, C. T.; Peden, C. H. F. Oxygen Vacancies and Catalysis on Ceria Surfaces. *Science* **2005**, *309*, 713−714.
(9) Karakoti, A. S.; Singh, S.; Kumar, A.; Malinska, M.; Kuchibhatla, S. V. N. T.; Wozniak, K.; Self, W. T.; Seal, S. PEGylated Nanoceria as Radical Scavenger with Tunable Redox Chemistry. *J. Am. Chem. Soc.* **2009**, *131*, 14144−14145.
(10) Pirmohamed, T.; Dowding, J. M.; Singh, S.; Wasserman, B.; Heckert, E.; Karakoti, A. S.; King, J. E. S.; Seal, S.; Self, W. T. Nanoceria Exhibit Redox State-Dependent Catalase Mimetic Activity. *Chem. Commun.* **2010**, *46*, 2736−2738.
(11) Korsvik, C.; Patil, S.; Seal, S.; Self, W. T. Superoxide Dismutase Mimetic Properties Exhibited by Vacancy Engineered Ceria Nanoparticles. *Chem. Commun.* **2007**, *46*, 1056−1058.
(12) Chen, J. P.; Patil, S.; Seal, S.; McGinnis, J. F. Rare Earth Nanoparticles Prevent Retinal Degeneration Induced by Intracellular Peroxides. *Nat. Nanotechnol.* **2006**, *1*, 142−150.
(13) Asati, A.; Santra, S.; Kaittanis, C.; Nath, S.; Perez, J. M. Oxidase-Like Activity of Polymer-Coated Cerium Oxide Nanoparticles. *Angew. Chem., Int. Ed.* **2009**, *48*, 2308−2312.
(14) Hirst, S. M.; Karakoti, A. S.; Tyler, R. D.; Sriranganathan, N.; Seal, S.; Reilly, C. M. Anti-Inflammatory Properties of Cerium Oxide Nanoparticles. *Small* **2009**, *5*, 2848−2856.
(15) Menchón, C.; Martín, R.; Apostolova, N.; Victor, V. M.; Álvaro, M.; Herance, J. R.; García, H. Gold Nanoparticles Supported on Nanoparticulate Ceria as a Powerful Agent against Intracellular Oxidative Stress. *Small* **2008**, *8*, 1895−1903.
(16) Pinna, A.; Lasio, B.; Piccinini, M.; Marmiroli, B.; Amentisch, H.; Falcaro, P.; Tokudome, Y.; Malfatti, L.; innocenzi, P. Combining Top-Down and Bottom-Up Routes for Fabrication of Mesoporous Titania Films Containing Ceria Nanoparticles for Free Radical Scavenging. *ACS Appl. Mater. Interfaces* **2013**, *5*, 3168−3175.
(17) Sayle, T. X. T.; Parker, S. C.; Sayle, D. C. Shape of CeO_2 Nanoparticles Using Simulated Amorphisation and Recrystallisation. *Chem. Commun.* **2004**, 2438−2439.
(18) Deshpande, S.; Patil, S.; Kuchibhata, S. V. N. T.; Seal, S. Size Dependency Variation in Lattice Parameter and Valency States in Nanocrystalline Cerium Oxide. *Appl. Phys. Lett.* **2005**, *87*, 133113.
(19) Cargnello, M.; Jaen, J. J. D.; Garrido, J. C. H.; Bakhmutsky, K.; Montini, T.; Gamez, J. J. C.; Gorte, R. J.; Fornasiero, P. Exceptional Activity for Methane Combustion over Modular Pd@CeO_2 Subunits on Functionalized Al_2O_3. *Science* **2012**, *337*, 713−717.
(20) Zhou, G.; Barrio, L.; Agnoli, S.; Senanayake, S. D.; Evans, J.; Kubacka, A.; Estrella, M.; Hanson, J. C.; Martinez-Arias, A.; Fernandez-Garcia, M.; Rodriguez, J. A. High Activity of $Ce_{1-x}Ni_xO_{2-y}$ for H_2 Production through Ethanol Steam Reforming: Tuning Catalytic Performance through Metal−Oxide Interactions. *Angew. Chem., Int. Ed.* **2010**, *49*, 9680−9684.
(21) Gionco, C.; Paganini, M. C.; Agnoli, S.; Reeder, A. E.; Giamello, E. Structural and Spectroscopic Characterization of CeO_2−TiO_2 Mixed Oxides. *J. Mater. Chem. A* **2013**, *1*, 10918−10926.
(22) Chen, L.; Si, Z.; Wu, X.; Wenig. DRIFT Study of CuO−CeO_2−TiO_2 Mixed Oxides for NO_x Reduction with NH_3 at Low Temperatures. *ACS Appl. Mater. Interfaces* **2014**, *6*, 8134−8145.
(23) Graciani, J.; Plata, J. J.; Sanz, J. F.; Liu, P.; Rodriguez, J. A. A Theoretical Insight into the Catalytic Effect of a Mixed-Metal Oxide at the Nanometer Level: The Case of the Highly Active Metal/CeO_x/TiO_2(110) Catalysts. *J. Chem. Phys.* **2010**, *132*, 104703.
(24) Agnoli, S.; Reeder, A. E.; Senanayake, S. D.; Hrbek, J.; Rodriguez, J. A. Structure and Special Chemical Reactivity of Interface-Stabilized Cerium Oxide Nanolayers on TiO_2(110). *Nanoscale* **2014**, *6*, 800−810.
(25) Park, J. B.; Graciani, J.; Evans, J.; Stacchiola, D.; Ma, S. G.; Liu, P.; Nambu, A.; Sanz, J. F.; Hrbek, J.; Rodriguez, J. A. High Catalytic Activity of Au/CeO_x/TiO_2(110) Controlled by the Nature of the Mixed-Metal Oxide at the Nanometer Level. *Proc. Natl. Acad. Sci. U. S. A.* **2009**, *106*, 4975−4980.
(26) Abbott, H. L.; Uhl, A.; Baron, M.; Lei, Y.; Meyer, R. J.; Stacchiola, D.; Bondarchuk, O.; Shaikhutdinov, S.; Freund, H. J. Relating Methanol Oxidation to the Structure of Ceria-Supported Vanadia Monolayer Catalysts. *J. Catal.* **2010**, *272*, 82−91.
(27) Wei, S.; Wang, Q.; Zhu, J.; Sun, L.; Line, H.; Guo, Z. Multifunctional Composite Core−Shell Nanoparticles. *Nanoscale* **2011**, *3*, 4474−4502.
(28) Gao, J.; Gu, H.; Xu, B. Multifunctional Magnetic Nanoparticles: Design, Synthesis, and Biomedical Applications. *Acc. Chem. Res.* **2009**, *42*, 1097−1107.
(29) Correa, D. N.; Silva, J. M. D. E.; Santos, E. B.; Sigoli, F. A.; Souza, A. G.; Mazali, I. O. TiO_2- and CeO_2-Based Biphasic Core−Shell Nanoparticles with Tunable Core Sizes and Shell Thicknesses. *J. Phys. Chem. C* **2011**, *115*, 10380−10387.
(30) Sutara, F.; Cabala, M.; Sedlacek, L.; Skala, T.; Skoda, M.; Matolin, V.; Prince, K. C.; Chab, V. Epitaxial Growth of Continuous CeO_2(111) Ultra-Thin Films on Cu(111). *Thin Solid Films* **2008**, *516*, 6120−6124.
(31) In Figure 2 the doublets used to fit the Ce 3d experimental photoemission line are labeled with the same color. For each doublet, the peaks pertaining to the same electronic configuration and related by spin orbit splitting have the same fwhm and their integrated intensity is fixed to the theoretical value of spin−orbit degeneracy (3:2).
(32) Reddy, B. M.; Khan, A.; Yamada, Y.; Kobayashi, T.; Loridant, S.; Volta, J. C. Structural characterization of CeO_2-MO_2 (M = Si^{4+}, Ti^{4+}, and Zr^{4+}) mixed oxides by Raman spectroscopy, X-ray photoelectron spectroscopy, and other techniques. *J. Phys. Chem. B* **2003**, *107*, 11475−11484.
(33) Yakovlev, V. V.; Scarel, G.; Aita, C. R.; Mochizuki, S. Short-range order in ultrathin film titanium dioxide studied by Raman spectroscopy. *Appl. Phys. Lett.* **2000**, *76*, 1107−1109.
(34) Lin, J.; Yu, J. C. An investigation on photocatalytic activities of mixed TiO_2-rare earth oxides for the oxidation of acetone in air. *J. Photochem. Photobiol., A* **1998**, *116*, 63−67.
(35) Hadjiivanov, K. I.; Klissurski, D. G. Surface chemistry of titania (anatase) and titania-supported catalysts. *Chem. Soc. Rev.* **1996**, *25*, 61−69.
(36) Martos, M.; Julian-Lopez, B.; Vicente Folgado, J.; Cordoncillo, E.; Escribano, P. Sol-gel synthesis of tunable cerium titanate materials. *Eur. J. Inorg. Chem.* **2008**, 3163−3171.
(37) Manea, F.; Houillon, F. B.; Pasquato, L.; Scrimin, P. Nanozymes: Gold-Nanoparticle-Based Transphosphorylation Catalysts. *Angew. Chem., Int. Ed.* **2004**, *43*, 6165−6169.
(38) Heckert, E. G.; Karakoti, A. S.; Seal, S.; Self, W. T. The Role of Cerium Redox State in the SOD Mimetic Activity of Nanoceria. *Biomaterials* **2008**, *29*, 2705−2709.
(39) Peng, Y. F.; Chen, X. J.; Yi, G. S.; Gao, Z. Q. Mechanism of the Oxidation of Organic Dyes in the Presence of Nanoceria. *Chem. Commun.* **2011**, *47*, 2916−2918.
(40) Gao, L. Z.; Zhuang, J.; Nie, L.; Zhang, J. B.; Zhang, Y.; Gu, N.; Wang, T. H.; Feng, J.; Yang, D. J.; Perrett, S.; Yan, X. Intrinsic Peroxidase-Like Activity of Ferromagnetic Nanoparticles. *Nat. Nanotechnol.* **2007**, *2*, 577−583.
(41) Chen, W.; Chen, J.; Liu, A. L.; Wang, L. M.; Li, G. W.; Lin, X. H. Peroxidase-Like Activity of Cupric Oxide Nanoparticle. *ChemCatChem* **2011**, *3*, 1151−1154.
(42) Dai, Z. H.; Liu, S. H.; Bao, J. C.; Jui, H. X. Nanostructured FeS as a Mimic Peroxidase for Biocatalysis and Biosensing. *Chem.—Eur. J.* **2009**, *15*, 4321−4326.
(43) Dutta, A. K.; Maji, S. K.; Srivastava, S. N.; Mondal, A.; Biswas, P.; Paul, P.; Adhikary, B. Synthesis of FeS and FeSe Nanoparticles from a Single Source Precursor: a Study of Their Photocatalytic

Activity, Peroxidase-Like Behavior, and Electrochemical Sensing of H_2O_2. *ACS Appl. Mater. Interfaces* **2012**, *4*, 1919−1927.
(44) Song, Y. J.; Qu, K. G.; Zhao, C.; Ren, J. S.; Qu, X. J. Graphene Oxide: Intrinsic Peroxidase Catalytic Activity and Its Application to Glucose Detection. *Adv. Mater.* **2010**, *22*, 2206−2210.
(45) Reeder, A. E.; Agnoli, S.; Rizzi, G.; Granozzi, G. Zr_2O_3 Nanostripes on TiO_2(110) Prepared by UHV Chemical Vapor Deposition. *J. Phys. Chem. C* **2014**, *118*, 8026−8033.
(46) Artiglia, L.; Agnoli, S.; Vittadini, A.; Verdini, A.; Cossaro, A.; Floreano, L.; Granozzi, G. Atomic Structure and Special Reactivity Toward Methanol Oxidation of Vanadia Nanoclusters on TiO_2(110). *J. Am. Chem. Soc.* **2013**, *135*, 17331−17338.
(47) Ganduglia-Pirovano, M. V.; Popa, C.; Sauer, J.; Abbott, H.; Uhl, A.; Baron, M.; Stacchiola, D.; Bondarchuk, O.; Shaikhutdinov, S.; Freund, H. J. Role of Ceria in Oxidative Dehydrogenation on Supported Vanadia Catalysts. *J. Am. Chem. Soc.* **2010**, *132*, 2345−2349.
(48) Artiglia, L.; Agnoli, S.; Savio, L.; Pal, J.; Celasco, E.; Rocca, M. A.; Bondino, F.; Magnano, E.; Castellarin-Cudia, C.; Netzer, F. P.; Granozzi, G. From Vanadia Nanoclusters to Ultrathin Films on TiO_2(110): Evolution of the Yield and Selectivity in the Ethanol Oxidation Reaction. *ACS Catal.* **2014**, *4*, 3715−3723.
(49) Chen, J.; Hu, P. Brønsted−Evans−Polanyi Relation of Multistep Reactions and Volcano Curve in Heterogeneous Catalysis. *J. Phys. Chem. C* **2008**, *112*, 1308−1311.
(50) Lin, J.-L.; Wheeldon, I. Kinetic Enhancements in DNA−Enzyme Nanostructures Mimic the Sabatier Principle. *ACS Catal.* **2013**, *3*, 560−564.